Room temperature synthesis of 3D-nanocrystalline graphitic carbon from biomass-derived sugars, alcohols, and polyphenolic compounds

We present an efficient method for synthesizing nanocrystalline carbon with sp^2/sp^3 hybridization using monosaccharides, disaccharides, alcohols, and polyphenolic compounds as carbon sources. The room-temperature electrochemical reduction of biomass-derived oxygenates occurs in an electrolyte solution comprising $[BMIM]^+[BF_4]^-$, H_2O_2, and water. This process employs negatively charged Ag cluster electrocatalysts on a Cu substrate, resulting in nanostructured carbon products within a relatively short reaction time.

ROYAL SOCIETY OF CHEMISTRY

rsc.li/nanoscale-advances

Check for updates

Room temperature synthesis of 3D-nanocrystalline graphitic carbon from biomass-derived sugars, alcohols, and polyphenolic compounds†

Wiyanti Fransisca Simanullang,[abc] Rungkiat Nganglumpoon,[ad] Suthasinee Watmanee,[ad] Piriya Pinthong,[ad] Weerachon Tolek,[ad] Yan Liu [ID][e] and Joongjai Panpranot [ID] *[adf]

Nanocrystalline carbon materials exhibit promising potential for sustainable and high-performance applications in electronics, energy storage, and environmental technologies. While sugars are abundant and renewable, converting them to graphitic carbon usually requires high temperature treatment. Here, we present a groundbreaking approach for synthesizing nanocrystalline carbon from readily available sugars such as glucose, fructose, and sucrose at ambient pressure and temperature. This novel method involves electrochemical reduction on a negatively charged Ag surface coupled with intermolecular dehydration between the organic precursors. By applying relatively low potentials ranging from -1.2 to -1.6 V *vs.* Ag/AgCl, and with the presence of hydrogen peroxide, oxygenic carbon precursors are efficiently transformed into nanocrystalline hybrid carbon structures. The role of hydrogen peroxide is pivotal in expediting hydrogen abstraction and facilitating the formation of 3D-nanostructured carbon allotropes. Characterization results based on Raman spectroscopy, transmission electron microscopy-energy dispersive X-ray spectroscopy-selected area electron diffraction (TEM-EDX-SAED), X-ray photoelectron spectroscopy (XPS), and grazing incidence-X-ray diffraction (GI-XRD) confirm the presence of mixed nanocrystalline sp^2–sp^3 hybridization in the resulting carbon materials. Moreover, this method's versatility extends beyond sugars to include alcohols, polyols, and polyphenolic compounds like ethanol, glycerol, and tannic acid, broadening its potential for biomass valorization.

Introduction

The widespread use of carbon nanomaterials as a central component for optics, electronics, bioengineering, agriculture, catalysts, and even renewable energy has received widespread attention. Due to its potential and natural abundance, biomass has been widely studied.[1–3] Carbon nanomaterials such as graphene,[4–6] nanodiamond, carbon allotropes, carbon nanotubes, *etc.*[7] have been synthesized from biomass.[8] However, the existing methods normally require high-energy processes, *i.e.*, chemical vapor deposition (CVD),[9] solvothermal reaction,[10] pyrolysis,[11] and laser ablation.[12] Therefore, developing a more efficient and environmentally friendly low-energy consumption process is imperative yet challenging.

In order to produce nanocrystalline carbon from biomass, an extremely high amount of energy is consumed.[13] For instance, wood,[14,15] carbohydrates,[16,17] agriculture residue,[18] *etc.* have been reported to have been used in hydrothermal and pyrolysis processes at a relatively high temperature and pressure. The established work showed that the synthesis of carbohydrate-derived carbon materials required heating at at least 200 °C for the hydrothermal process and up to 1000 °C for the pyrolysis and thermal processes while at 180–200 °C for the hydrothermal process with a quite long reaction time (summarized in Table 1). Nevertheless, due to their ability to enable C–C coupling *via* intermolecular dehydration, the utilization of alcoholic compounds such as ethanol and sugars such as glucose to synthesize crystalline sp^3 carbon allotropes has been achieved under much lower energy consumption. To illustrate this, n-diamond nanocrystals were grown by ultrasonically

[a]Center of Excellence on Catalysis and Catalytic Reaction Engineering, Department of Chemical Engineering, Faculty of Engineering, Chulalongkorn University, Bangkok 10330, Thailand. E-mail: joongjai.p@chula.ac.th

[b]Research Center for Chemistry, National Research and Innovation Agency, Jakarta 10340, Indonesia

[c]Department of Chemical Engineering, Faculty of Engineering, Widya Mandala Surabaya Catholic University, Surabaya 60112, Indonesia

[d]CrystalLyte Co., Ltd., Research Unit 904, Faculty of Engineering, Chulalongkorn University, Bangkok, 10330, Thailand

[e]Catalysis & Green Process Engineering Division, Institute of Sustainability for Chemicals, Energy and Environment, Agency for Science, Technology and Research, 1 Pesek Road, Jurong Island, Singapore 627833

[f]Bio-Circular-Green-economy Technology & Engineering Center (BCGeTEC), Department of Chemical Engineering, Faculty of Engineering, Chulalongkorn University, Bangkok, Thailand 10330

† Electronic supplementary information (ESI) available. See DOI: https://doi.org/10.1039/d4na00440j

Table 1 Summary of graphitic carbon synthesis from sugars

Entry	Methodology	Catalyst	Sugar amount (g)	T (°C)	t (h)	Ref.
1	Single-compartment electrolysis	Ag	16.20	25 (RT)	0.5	This work
2	Hydrothermal	Guanine	0.075	1000	2	16
3	High pressure	—	—	—	24	17
4	Hydrothermal	—	0.04	200	6	19
5	Hydrothermal	—	6.17	250	6	20
6	Pyrolysis	$Fe(NO_3)_3$	20.00	—	24	21
7	Pyrolysis	$Fe(NO_3)_3$	5.00	1000	1	22
8	Hydrothermal	—	0.27	180	6	23
9	Thermal synthesis	—	2	550	4	24
10	Thermal synthesis	—	3	900	3	25
11	Microwave-assisted polymerization	—	5	550	0.35	26
12	Hydrothermal	—	4.00	220	12	27
13	Hydrothermal	—	3.60	180	18	28
14	Pyrolysis	$Fe(NO_3)_3$	5.00	800	1	29

treating KOH ethanol at room temperature followed by adding HCl to terminate the process of crystallization.[30] However, the reaction governing the process is generally long and the separation problem also arises. These issues need to be addressed to improve the process.

Our latest contributions reported that the 3D-nanostructured carbon allotropes grew from gaseous CO_2 under CO_2 electrochemical reduction (CO_2RR).[31,32] Nanocrystalline carbon displaying more than 96% selectivity and ~1 μm thickness was obtained at relatively low applied potentials between −1.1 and −1.6 V vs. Ag/AgCl. The negatively charged nascent Ag nanoclusters formed during the CO_2RR reportedly have a high catalytic performance and stability. In this system, CO_2 was purged continuously into the electrolyte solution during the reaction. The CO_2RR was then applied for nano-graphene production using Bi deposited on Sn as an electro-catalyst. Similarly, the formation of negatively charged nascent Bi clusters led to the growth of nanocrystalline carbon.[33] More recently, we reported nanodiamond formation with an average size of 27 nm by electrochemical reduction of acetic acid on Ag/Cu prepared via in situ ion electrodeposition.[34] The formation amount of negatively charged nascent Ag on the Cu foil from the ultra-small amount of Ag^+ cations in the presence of the N^+-stabilizing system played an essential role in nanocrystalline carbon production. These findings indicate that negatively charged nascent metal clusters are essential.

In this study, the coupling effects between intermolecular dehydration and catalysis on negatively charged metal nano-clusters to accelerate sp^2–sp^3 nanocrystalline carbon formation under ambient conditions can be induced via the utilization of organic precursors having the ability to perform intermolecular dehydration, which include sugars, alcoholic compounds, and polyphenolic compounds in the adaptive electrochemical system with the assistance of H_2O_2 as a hydrogen abstractor for unpaired hydrogen atoms.[35,36] To elaborate, electrochemical reduction was applied to various types of sugars, alcoholic compounds, and polyphenolic compounds on the electro-chemically induced negatively charged nascent Ag in an aqueous electrolyte. The as-synthesized 3D-nanostructured graphitic carbon contains both sp^2 and sp^3 hybridization.

Experimental

Ag-electrocatalyst preparation

To prepare Ag/Cu as an electrocatalyst, Cu foil (Alfa Aesar, 99.9999%) was polished using 800-grit sandpaper until it was visibly smooth and had a thickness of 0.1 mm. The Ag-electrocatalysts were created through an electrochemical deposition, utilizing a two-electrode setup featuring a copper substrate cathode and a platinum rod anode. The electrolyte solution was a mixture of 0.01 M $AgNO_3$ and 0.6 M $(NH_4)_2SO_4$. The electrocatalyst was deposited onto the substrate in a square shape with a working area of 1 cm^2 by immersing the substrate in the electrolyte solution and applying a constant electrical potential of −1.1 V for 20 seconds. The sample was then washed with deionized (DI) water and dried overnight at room temperature before being used. All materials used in the experiment were purchased from Sigma-Aldrich and were not further purified.

Carbon nanostructure deposition

Carbon species were deposited using a potentiostat (Multi Autolab (M204), Metrohm) in a beaker-type reactor equipped with a three-electrode system under an air atmosphere. The working electrode was the Ag electrocatalyst produced using the electrochemical deposition process. The reference electrode was Ag/AgCl, while the counter electrode was a 50 mm × 50 mm Pt plate. The electrolyte solution had a molarity ratio of 4 : 20 : 3 of $[BMIM]^+[BF_4]^-$/carbohydrate/H_2O_2 diluted in 45 cm^3 deionized water. The electrochemical reduction of different types of sugars and alcohols was carried out using a potentiostat in a beaker-type reactor equipped with a three-electrode system at room temperature for 30 min. To determine the right electrical potential applied to each type of sugar, cyclic voltammetry (CV) was performed, where a trial and error procedure at more negative potentials than the onset potential from the CV was

used. The measurement was done by scanning the applied potential from 2 to −2 V *vs.* Ag/AgCl on the Cu substrate in the presence of the Ag-electrocatalyst. The potentials applied for all carbon sources are −1.2 V, −1.4 V, and −1.6 V *vs.* Ag/AgCl. After the electrochemical reaction, the working electrodes were collected, washed with DI water, and further analyzed. All chemicals were purchased from Sigma-Aldrich without purification.

Characterization

Raman spectra were recorded using a PerkinElmer Spectrum GX with a UV line at 532 nm, a TE-cooled CCD detector, and a laser power output of 10 milliwatts. Fityk software was used to determine peak parameters and ratios through deconvolution.[37] The solid product morphologies were examined using SEM-EDX analysis (JEOL JSM-5800LV), while TEM with EDX and SAED was performed with a JEOL JEM-2010. The TEM-EDX-SAED samples were prepared by dissolving the product in ethanol, dropping a few drops of the resulting suspension on the TEM grid, and then examining the samples with an FEI TECNAI G2 Spirit Twin. Focused ion beam field emission scanning electron microscopy (FIB-SEM) was conducted on an FEI Versa 3D. XPS spectra were obtained on an Amicus spectrometer using 10 kV and 20 mA Mg K$_\alpha$ X-ray radiation to analyze the element states of the electrocatalysts. Thin films were analyzed by GIXRD at an incident angle of 3° at 12 keV (wavelength of 0.103 nm) concerning the substrate surface, and Cu K (wavelength 0.154 nm) was used to calculate the results. The study was conducted at the Synchrotron Light Research Institute (Public Organization) BL 7.2W beamline at the Synchrotron Thailand Central Lab. Electrochemical Impedance Spectroscopy (EIS) was performed in the frequency range 0.1 MHz to 0.001 Hz using a potentiostat (Multi Autolab (M204), Metrohm).

Results and discussion

To demonstrate the system, fructose was utilized as a carbon source in the process with the Ag/Cu electrode at the applied potential of −1.6 V *vs.* Ag/AgCl for 30 min. For comparison, the Ag electrocatalyst was also tested in the electrolyte solution at −1.6 V *vs.* Ag/AgCl without sugar. After proceeding through the reaction, the cathode was washed with DI water to remove the remnant electrolyte before further characterization by Raman spectroscopy, GI-XRD, and SEM-EDX (Fig. 1). While the dendritic structure of Ag particles finely deposited on Cu foil was retained, both Raman spectra and GIXRD showed no carbon species when the reaction was carried out without sugar. A significant amount of carbon was observed on the used
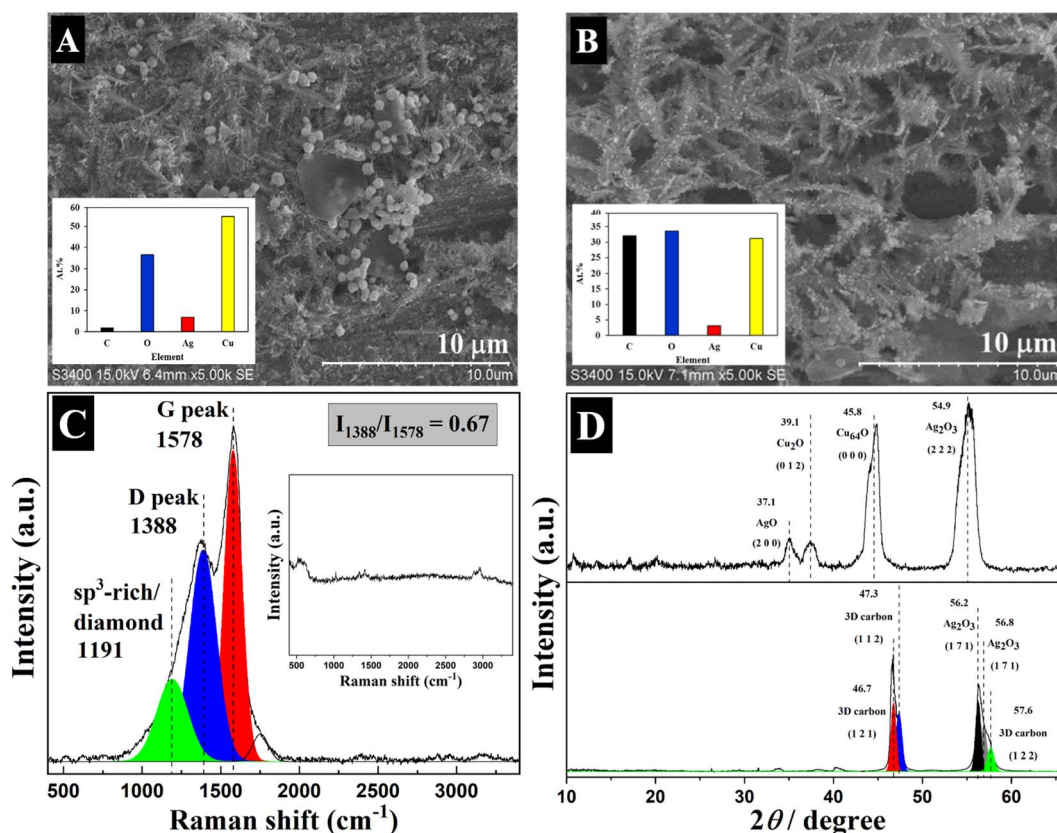

Fig. 1 The SEM–EDX results of Ag/Cu electrocatalysts before (A) and after (B) electrochemical reduction, (C) Raman results of the electrodes after electrochemical reduction (inset = electrode after reaction in the absence of sugar), and (D) GIXRD results of the electrodes before (upper) and after (lower) electrochemical reduction. Fructose was used as the carbon source in the reaction in the presence of H_2O_2 at −1.6 V *vs.* Ag/AgCl for 30 min.

electrode (>30% at.) after the reaction with fructose, which accounts for a C : Ag atomic ratio of 13. These characterization results indicate that the carbon species were originally from sugars as a carbon source. Moreover, Raman spectra of the electrodes after reaction with fructose exhibit several peaks of nanocrystalline carbon structures containing both sp^2 and sp^3 hybridization states. The D and G bands were detected at 1388 and 1578 cm^{-1}, respectively. These bands correspond to the breathing mode of the sp^2 carbon atoms in rings likely arising from the defect in the structure such as heteroatoms or sp^3 carbon atoms, which are bonded to the sp^2 carbon atoms, and the bond stretching of sp^2 carbon atoms, respectively. The presence of D and G bands confirms the presence of sp^2 carbon domains in the structure. Meanwhile, the incorporation of sp^3 hybridized carbon in the nanocrystalline structure was demonstrated by the observation of Raman peaks at 1191 cm^{-1}. The high FWHM of the D band indicates the development of the graphitic structure, and the ratio intensity of the D and G bands (I_D/I_G) is a good indicator of the graphitization degree. Results suggested that well-ordered nanocrystalline graphite was obtained.[38–40] The size of the crystalline graphite (L_a) can be estimated from the I_D/I_G ratio using the equation: $L_a = (I_D/I_G)/C(\lambda)$, where $C(\lambda) \approx 2.4 \times 10^{-10}\lambda$, where λ is the Raman excitation wavelength (532 nm) and the calculated crystalline domain size is 185 nm.[41] The GIXRD results also comply with Raman showing several main peaks of the 3D carbon structure indexed to the (121), (112), and (122) planes of the so-called "Diamond-C" located at 2θ angles of 46.7°, 47.3° and 57.6°, respectively. Diamond-C is a 3D progressive intermediate for the transformation of graphite to diamond, thus being a mixed sp^2/sp^3 crystalline solid carbon phase.[42,43]

In addition to fructose, other sugars, alcohols, and polyphenolic compounds including glucose, sucrose, ethanol, glycerol, and tannic acid were successfully applied to the process as revealed by Raman spectra which show peaks relating to sp^2 and sp^3 hybridized carbon as shown in Fig. 2. The effect of H_2O_2 in the electrolyte solution on the reducibility of sugars is also demonstrated. The results of electrochemical reduction over sugars and alcohols without H_2O_2 are shown in Fig. 2 (inset). D and G peaks were detected for both fructose and glucose whereas there were no peaks for sucrose. This indicates that fructose and glucose are more manageable to reduce than the others. Without H_2O_2, fructose still showed a clear I_D/I_G ratio. This is due to the higher stability of the open chain in a fructose (ketohexose) solution compared to glucose (aldohexose). The presence of H_2O_2 can significantly enhance the formation of sp^2/sp^3 hybridized carbon due to its ability to accelerate intermolecular dehydration *via* hydrogen abstraction. Here, the geometry and the atomic partial charges along with the electronegativities of the monosaccharides play the main role. Its structure–property relationship was found to be the significant factor in the solubility (0.0735 and 0.0944 mole fraction (mol/mol) for fructose and glucose, respectively.[44] Besides, the open-chain (pyranose form) present in the aldehyde/ketone might possibly undergo reduction.[45] They can be transformed into carbon allotropes without adding hydrogen peroxide. Meanwhile, when larger molecules such as disaccharides (*e.g.*, sucrose) are used as the carbon source, carbon allotropes' formation requires hydrogen peroxide to abstract hydrogen and hydrolyze the glycosidic linkage between monosaccharides. A similar trend was observed for the other carbon sources. However, it should be noted that in general,
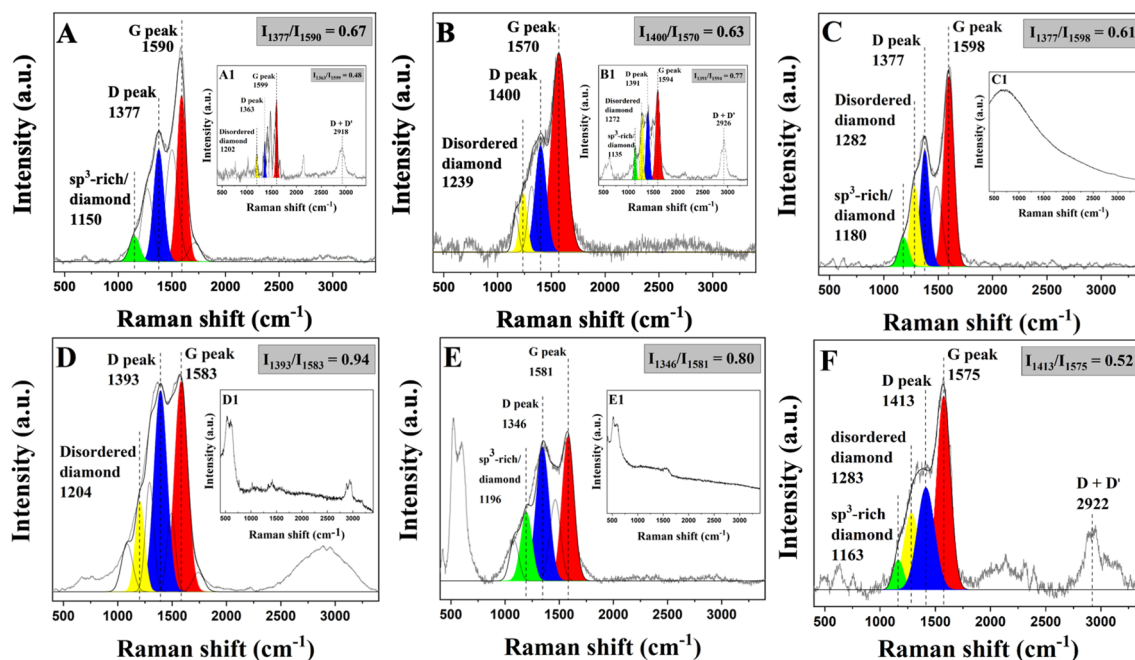

Fig. 2 Raman spectra of electrochemical reduction of sugars in the presence and absence (inset) of H_2O_2: fructose (A), glucose (B), sucrose (C), ethanol (D), glycerol (E), tannic acid (F).

carbohydrates in polymer form such as starch and cellulose are not highly soluble in water, which is the main solvent in our system, thus not being able to be utilized in the process.

The electrode area was considered to calculate the total geometric current density (mA cm^{-2}) from the potentiostat, as shown in Fig. 3A. In the presence of H_2O_2, the electrochemical reduction of sugars is quite stable during a 30 min reaction with a relatively high current especially for glucose and fructose, which corresponds to the conversion of sugars into carbon materials. In the electrolyte solution without sugar, the current density swung from the beginning to the end at a high value due to the H_2 evolution reaction. In the process, H_2O_2 decomposes into hydroxyl radicals in the system and these hydroxyl radicals play a crucial role as a hydrogen abstractor, encouraging an intermolecular dehydration process in the formation of carbon from the carbon sources. Electrochemical impedance spectroscopy was employed to investigate the charge transfer resistance (R_{ct}) on the electrochemical reduction of sugars and the results are shown in Fig. 3B. A semicircle of Nyquist plots indicates the charge transfer of electrons in the system. In the presence of sugars in the electrolyte solution, 2.3 Ω and 2.5 Ω were obtained for fructose and sucrose, respectively. This number is higher than in the absence of sugar at 2.1 Ω.

TEM-EDX-SAED (Fig. 4) further characterizes the formation of nanostructured carbon materials. The TEM images show that the as-synthesized carbon products are crystalline in nature by showing obvious fringes in the structure with high at% of carbon of 75% as revealed by EDX. The corresponding SAED patterns show obvious bright spots matching Diamond-C (111) and graphite (002), (101), (102), (211), and (015) planes. Moreover, from the XPS results (Fig. 5), sp C–C, sp^2 C–C, and sp^3 C–C were present at binding energies of 282.8, 284.8, and 285.9 eV, respectively, in good agreement with the carbon materials hybridization as reported in the literature.[46,47] The percentage of sp^3 hybridized carbon in the structure from XPS results is 32.7%.

The effect of applied potential on the formation of carbon in our system was investigated using fructose, glucose, and sucrose as the carbon source and the results are shown in Fig. 6. For fructose and glucose, there were no carbon products formed on the electrode when the applied potential of −1.2 V vs. Ag/AgCl was used, as revealed by the Raman spectra of the electrodes. The formation of carbon on the cathode gradually occurred upon increasing the applied potential to −1.4 V and further improved upon elevating the applied potential to −1.6 V, as shown by the significantly higher intensity of carbon characteristic peaks as compared to those at −1.4 V. Excess electrons mobilizing on the negatively charged Ag surface may enhance the ability of Ag electrocatalysts to reduce the sugars. The optimum applied potentials for electrochemical reduction of fructose, glucose, and sucrose are determined to be −1.4 to −1.6 V vs. Ag/AgCl. However, a too high negative applied potential can cause the negative-bias fusion of Ag particles which may deactivate the function of the negatively charged Ag surface.

Upon applying the negative potential on the cathode, the excess electrons reduce Ag oxide thin film layers on the Ag electrocatalysts, resulting in the formation of negatively charged metal nanoclusters of Ag stabilized by the [BMIM]$^+$ cation.[31] Moreover, the room-temperature ionic liquid electrolyte controls the electrochemical reduction by its structural transition and water presence increases the dissociation of the ionic liquid, resulting in a higher amount of electrolyte ionic species. A complex of cation and organic precursors reduced the activation barrier for electron transfer and the overpotential might be cancelled. The presence of the anion and cation of [BMIM]$^+$[BF$_4$]$^-$ can stabilize the reduction reaction which allows reduction resistance at the electrode.[48–52] The reduction of the organic precursors into carbon atoms then occurred on the negatively charged Ag surface concurrently with the intermolecular dehydration between the molecules of organic precursors, which were accelerated by hydrogen abstraction from hydroxyl radicals decomposed from H_2O_2 in the system, resulting in the formation of sp^2/sp^3 hybridized crystalline carbon allotropes. In addition to the reductive power of the Ag electrocatalysts, the intermolecular dehydration highly
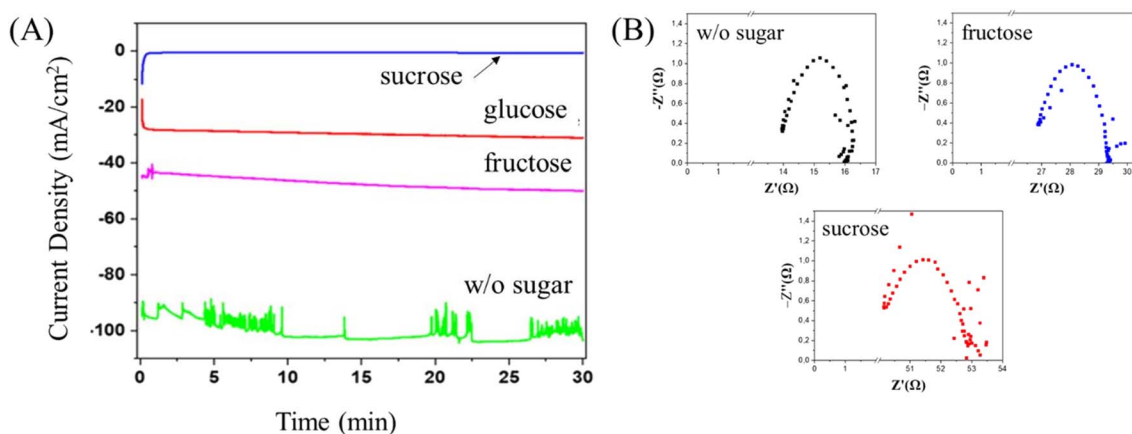

Fig. 3 Current density as a function of reaction time during the electrochemical reduction of sugars in the presence of H_2O_2 (A) and the charge transfer resistance (R_{ct}) on electrochemical reduction of sugars (B) in comparison to the reaction in the absence of sugar.
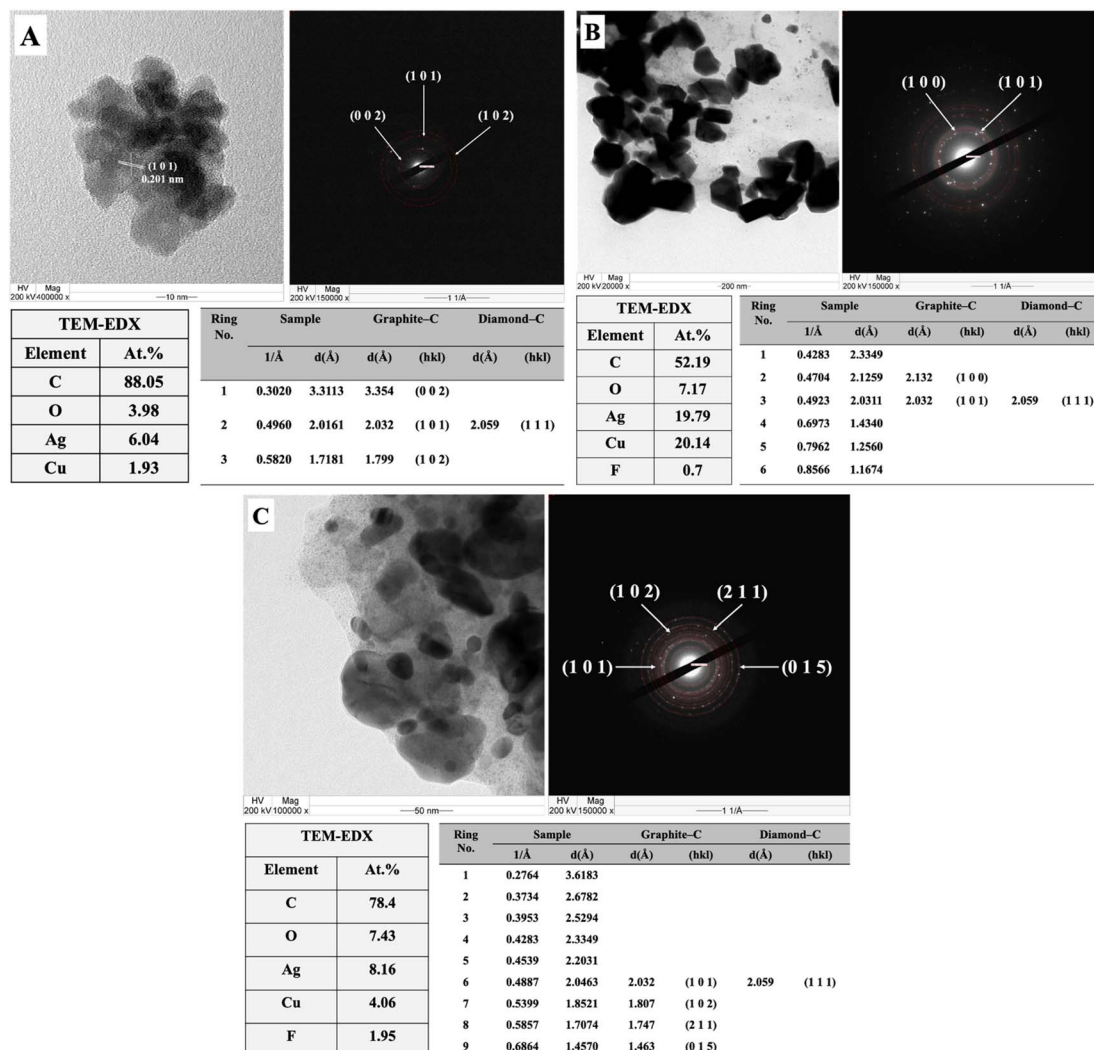
(A)

TEM-EDX

Element	At.%
C	88.05
O	3.98
Ag	6.04
Cu	1.93

Ring No.	Sample		Graphite–C		Diamond–C	
	1/Å	d(Å)	d(Å)	(hkl)	d(Å)	(hkl)
1	0.3020	3.3113	3.354	(0 0 2)		
2	0.4960	2.0161	2.032	(1 0 1)	2.059	(1 1 1)
3	0.5820	1.7181	1.799	(1 0 2)		

(B)

TEM-EDX

Element	At.%
C	52.19
O	7.17
Ag	19.79
Cu	20.14
F	0.7

Ring No.	Sample		Graphite–C		Diamond–C	
	1/Å	d(Å)	d(Å)	(hkl)	d(Å)	(hkl)
1	0.4283	2.3349				
2	0.4704	2.1259	2.132	(1 0 0)		
3	0.4923	2.0311	2.032	(1 0 1)	2.059	(1 1 1)
4	0.6973	1.4340				
5	0.7962	1.2560				
6	0.8566	1.1674				

(C)

TEM-EDX

Element	At.%
C	78.4
O	7.43
Ag	8.16
Cu	4.06
F	1.95

Ring No.	Sample		Graphite–C		Diamond–C	
	1/Å	d(Å)	d(Å)	(hkl)	d(Å)	(hkl)
1	0.2764	3.6183				
2	0.3734	2.6782				
3	0.3953	2.5294				
4	0.4283	2.3349				
5	0.4539	2.2031				
6	0.4887	2.0463	2.032	(1 0 1)	2.059	(1 1 1)
7	0.5399	1.8521	1.807	(1 0 2)		
8	0.5857	1.7074	1.747	(2 1 1)		
9	0.6864	1.4570	1.463	(0 1 5)		

Fig. 4 The TEM-EDX-SAED results of the carbon products obtained from the electrochemical reduction of (A) fructose, (B) glucose, and (C) sucrose on Ag/Cu electrocatalysts at −1.6 V vs. Ag/AgCl.
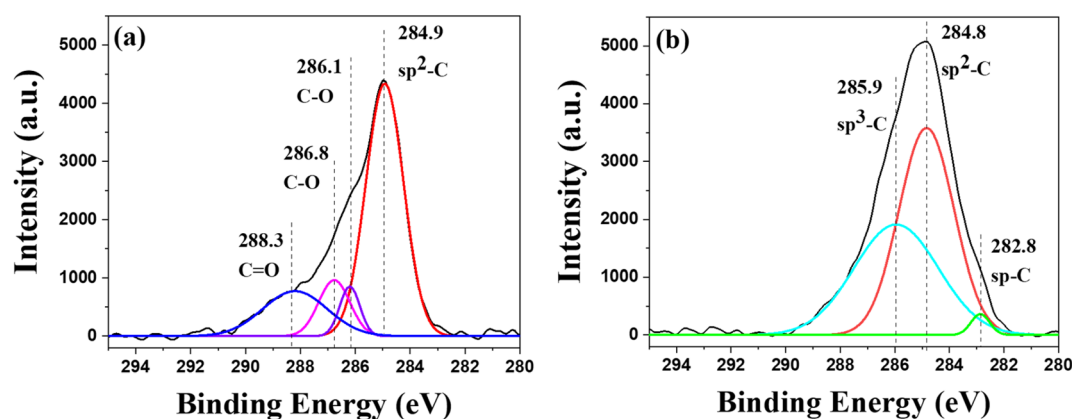

Fig. 5 Deconvoluted XPS spectra of the electrodes after electrochemical reduction of (a) electrolyte solution with the absence of sugar and (b) electrolyte solution with sugars on Ag/Cu.

contributed to the formation of nanocrystalline sp^2/sp^3 hybridized carbon. The presence of H_2O_2 can significantly enhance the formation of sp^2/sp^3 hybridized carbon due to its ability to accelerate intermolecular dehydration via hydrogen abstraction. Generally, the number of hydrogen atoms in this type of organic precursor is significantly higher than that of
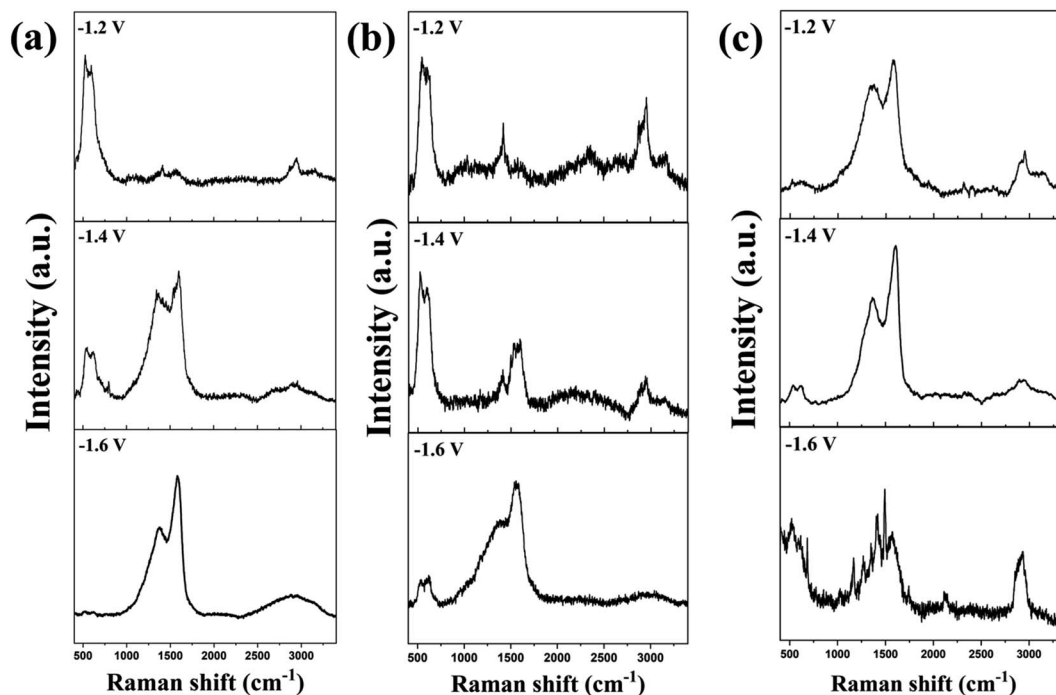
Fig. 6 Raman spectra of the Ag/Cu electrocatalyst after electrochemical reduction of fructose (a), glucose (b), and sucrose (c) at different applied potentials *vs.* Ag/AgCl.

hydroxyl groups, resulting in unpaired hydrogen atoms interfering with the formation of the carbon network. Hydroxyl radicals have been reported to be a hydrogen abstractor in the CVD process, forming carbon free radicals from C–H bonds, which eventually form C–C bonds to construct the carbon allotrope's structure.[53,54] H_2O_2 is known to generate hydroxyl radicals even under ambient conditions,[55] thus being appropriate for use as the hydrogen abstractor in the system. The significant role of H_2O_2 was confirmed for all carbon sources used in this work. It can be said that intermolecular dehydration accelerated by hydrogen abstraction plays a leading role in the formation of carbon products. Table 1 shows details of the recent reports of the development of graphitic carbon from sugars. The results confirm that the current research is more efficient than previous, state-of-the-art works.

Conclusions

We present a highly efficient approach for the synthesis of nanocrystalline carbon containing sp^2/sp^3 hybridization using monosaccharides, disaccharides, alcohols, and polyphenolic compounds as the carbon source. The room temperature electrochemical reduction of biomass-derived oxygenates takes place in an electrolyte solution consisting of $[BMIM]^+[BF_4]^-$, H_2O_2, and water using negatively charged Ag cluster electrocatalysts on a Cu substrate at a relatively short reaction time for producing nanostructure carbon products. 3D-nanostructured carbon was obtained from all types of carbon sources. In addition, the presence of sp^2/sp^3 hybridization was revealed. The highest carbon product deposition achieved on Ag/Cu is that of fructose, at nearly 90%. This novel approach may lead to

a sustainable room-temperature versatile method using naturally abundant biomass resources to produce nanocrystalline carbon products.

Data availability

Data for this article are available at the link **https://drive.google.com/drive/folders/1W46BBj3aJOZtptIbfoxa2W8c7UOWjhwK?usp=sharing**.

Conflicts of interest

There are no conflicts to declare.

Acknowledgements

References

1 E. Thompson, A. E. Danks, L. Bourgeois and Z. Schnepp, *Green Chem.*, 2015, **17**, 551–556, DOI: **10.1039/C4GC01673D**.
2 J. Shi, Y. Wang, W. Du and Z. Hou, *Carbon*, 2016, **99**, 330–337, DOI: **10.1016/j.carbon.2015.12.049**.

3 C. Wang, Y. Wang, J. Graser, R. Zhao, F. Gao and M. J. O'Connell, *ACS Nano*, 2013, **7**, 11156–11165, DOI: **10.1021/nn4048759**.

4 B. Gurzęda, P. Florczak, M. Kempiński, B. Peplińska, P. Krawczyk and S. Jurga, *Carbon*, 2016, **100**, 540–545, DOI: **10.1016/j/carbon.2016.01.044**.

5 K. Zhan, R. Zhao, F. Li, T. Wang, W. Mo, Z. Yang and B. Zhao, *J. Alloys Compd.*, 2021, **886**, 161228, DOI: **10.1016/j.jallcom.2021.161228**.

6 M. A. Ceniceros-Reyes, K. S. Marín-Hernández, U. Sierra, E. M. Saucedo-Salazar, R. Mendoza-Resendez, C. Luna, P. J. Hernández-Belmares, O. S. Rodríguez-Fernández, S. Fernández-Tavizón, E. Hernández-Hernández and E. D. Barriga-Castro, *Surf. Interfaces*, 2022, **35**, 102448, DOI: **10.1016/j.surfin.2022.102448**.

7 H. Wang, Z. Han, L. Zhang, C. Cui, X. Zhu, X. Liu, J. Han and Q. Ge, *J. CO_2 Util.*, 2016, **15**, 41–49, DOI: **10.1016/j.jcou.2016.04.013**.

8 K. Zhang, Z. Huang, M. Yang, M. Liu, Y. Zhou, J. Zhan and Y. Zhou, *SusMat*, 2023, **3**(5), 558–580, DOI: **10.1002/sus2.157**.

9 K. Hiratochi, D. Terada, H. Suga, M. Okada, K. Bando, T. Kodaira, T. Yamada, T. Shimizu, K. Saiki and T. Kubo, *Mater. Chem. Front.*, 2024, **8**, 814–823, DOI: **10.1039/D3QM00992K**.

10 S. Zhang, Y. Tian, M. Liu, T. Hong-Meng, C.-R. Li, X. Zeng, X. Xiao and C. Redshaw, *Mater. Chem. Front.*, 2022, **6**, 973–980, DOI: **10.1039/d2qm00022a**.

11 R. Zhang, J. R. Adsetts, Y. Nie, X. Sun and Z. Ding, *Carbon*, 2018, **129**, 45–53, DOI: **10.1016/j.carbon.2017.11.091**.

12 G. K. Yogesh, E. P. Shuaib, A. K. Priya, P. Rohini, S. V. Anandhan, U. M. Krishnan, V. Kalyanavalli, S. Shukla and D. Sastikumar, *Opt Laser. Technol.*, 2021, **135**, 106717, DOI: **10.1016/j.optlastec.2020.106717**.

13 H. He, R. Zhang, P. Zhang, P. Wang, N. Chen, B. Qian, L. Zhang, J. Yu and B. Dai, *Adv. Sci.*, 2023, **10**, 2205557, DOI: **10.1002/advs.202205557**.

14 F. Salvador, J. Sanchez-Montero and C. Izquierdo, *J. Phys. Chem. C*, 2007, **111**(37), 14011–14020, DOI: **10.1021/jp073723e**.

15 Y. Nakayasu, Y. Goto, Y. Katsuyama, T. Itoh and M. Watanabe, *Carbon Trends*, 2022, **8**, 100190, DOI: **10.1016/j.cartre.2022.100190**.

16 B. Huang, Y. Liu and Z. Xie, *J. Mater. Chem. A*, 2017, **5**, 23481–23488, DOI: **10.1039/C7TA08052B**.

17 X. Wang, X. Yang, Y. Wang, X. Tang, H. Zheng, P. Zhang, D. Gao, G. Che, Z. Wang, A. Guan, J.-F. Xiang, M. Tang, X. Dong, K. Li and H. Mao, *J. Am. Chem. Soc.*, 2022, **144**, 21837–21842, DOI: **10.1021/jacs.2c08914**.

18 M. Genovese, J. Jiang, K. Lian and N. Holm, *J. Mater. Chem. A*, 2015, **3**, 2903–2913, DOI: **10.1039/C4TA06110A**.

19 N. Papaioannou, A. Marinovic, N. Yoshisawa, A. E. Goode, M. Fay, A. Khlobystov, M.-M. Titirici and A. Sapelkin, *Sci. Rep.*, 2018, **8**(6559), 1–10, DOI: **10.1038/s41598-018-25012-8**.

20 P. Zhang, J. Fan, Y. Wang, Y. Dang, S. Heumann and Y. Ding, *Carbon*, 2024, **222**, 118998, DOI: **10.1016/j.carbon.2024.118998**.

21 J. Yang and S. Zuo, *Diamond Relat. Mater.*, 2019, **95**, 1–4, DOI: **10.1016/j.diamond.2019.03.018**.

22 L. Gai, J. Li, Q. Wang, R. Tian and K. Li, *J. Environ. Chem. Eng.*, 2021, **9**, 106678, DOI: **10.1016/j.jece.2021.106678**.

23 H. E. Emam, M. El-Shahat, A. K. Allayeh and H. B. Ahamed, *Biocatal. Agric. Biotechnol.*, 2023, **47**, 102577, DOI: **10.1016/j.bcab.2022.102577**.

24 A. Smykalová, E. Kinnertová, V. Slovák and P. Praus, *J. Taiwan Inst. Chem. Eng.*, 2024, **158**, 104864, DOI: **10.1016/j.jtice.2023.104864**.

25 S. Rawat, A. R. Kottaichamy, Z. M. Bhat, S. Hotha, M. O. Thotiyl and T. Bhaskar, *Biomass Convers. Biorefin.*, 2022, DOI: **10.1007/s13399-022-02671-2**.

26 X. Hou, L. Cui, H. Du, L. Gu, Z. Li and Y. Yuan, *Appl. Catal., B*, 2020, **278**, 119253, DOI: **10.1016/j.apcatb.2020.119253**.

27 S. Supajaruwong, S. Porahong, A. Wibowo, Y.-S. Yu, M. J. Khan, P. Pongchaikul, P. Posoknistakul, N. Laosiripojana, K. C-Wu and C. Sakdaronnarong, *Sci. Technol. Adv. Mater.*, 2023, **24**, 2260298, DOI: **10.1080/14686996.2023.2260298**.

28 P. Baruah, B. K. Das, M. Bora, B. K. Saikia and D. Mahanta, *Mater. Today Commun.*, 2022, **33**, 104219, DOI: **10.1016/j.mtcomm.2022.104219**.

29 R. D. Hunter, J. L. Rowlandson, G. L. Smales, B. R. Pauw, V. P. Ting, A. Kulak and Z. Schnepp, *Mater. Adv.*, 2020, **1**, 3281–3291, DOI: **10.1039/D0MA00692K**.

30 D. Dai, Y. Li and J. Fan, *Carbon*, 2021, **179**, 133–141, DOI: **10.1016/j.carbon.2021.04.038**.

31 R. Nganglumpoon, S. Watmanee, T. Teerawatananond, P. Pinthong, K. Poolboon, N. Hongrutai, D. N. Tungasmita, S. Tungasmita, Y. Boonyongmaneerat, N. Jantaping, S. Wannapaiboon, P. Praserthdam, Y. Morikawa, J. G. Goodwin and J. Panpranot, *Carbon*, 2022, **187**, 241–255, DOI: **10.1016/j.carbon.2021.11.011**.

32 S. Watmanee, R. Nganglumpoon, N. Hongrutai, P. Pinthong, P. Praserthdam, S. Wannapaiboon, P. Á. Szilágyi, Y. Morikawa and J. Panpranot, *Nanoscale Adv.*, 2022, **4**, 2255–2267, DOI: **10.1039/D1NA00876E**.

33 P. Pinthong, S. Phupaichitkun, S. Watmanee, R. Nganglumpoon, D. N. Tungasmita, S. Tungasmita, Y. Boonyongmaneerat, N. Promphet, N. Rodthongkum and J. Panpranot, *Nanomaterials*, 2022, **12**(19), 3389, DOI: **10.3390/nano12193389**.

34 N. Hongrutai, R. Nganglumpoon, S. Watmanee, P. Pinthong, P. Szilágyi, M. M. Titirici and J. Panpranot, *Mater. Today Chem.*, 2023, **30**, 101509, DOI: **10.1016/j.mtchem.2023.101509**.

35 X. Ren, X. Dong, L. Liu, J. Hao, H. Zhu, A. Liu and G. Wu, *SusMat*, 2023, **3**(3), 442–470, DOI: **10.1002/sus2.149**.

36 H. W. Kim, M. B. Ross, N. Kornienko, L. Zhang, J. Guo, P. Yang and B. D. Mccloskey, *Nat. Catal.*, 2018, **1**, 282–290, DOI: **10.1038/s41929-018-0044-2**.

37 L. F. Tomilin, S. V. Erohin, N. A. Nebogatikova, I. V. Antonova, A. K. Gutakovskii, V. A. Volodin, E. A. Korneeva and P. B. Sorokin, *Carbon*, 2024, **220**, 118832, DOI: **10.1016/j.carbon.2024.118832**.

38 M. A. Pimenta, G. Dresselhaus, M. S. Dresselhaus, L. G. Cançado, A. Jorio and R. Saito, *Phys. Chem. Chem. Phys.*, 2007, **9**, 1276–1290, DOI: **10.1039/B613962K**.

39 L. G. Cançado, K. Takai, T. Enoki, M. Endo, Y. A. Kim, H. Mizusaki, N. L. Speziali, A. Jorio and M. A. Pimenta, *Carbon*, 2008, **46**, 272–275, DOI: **10.1016/j.carbon.2007.11.015**.

40 W. Deng, T. Liu, H. Li, X. Liu, A. Dang, Y. Liu and H. Wu, *J. Colloid Interface Sci.*, 2022, **618**, 129–140, DOI: **10.1016/j.jcis.2022.03.071**.

41 K. Nagashima, M. Nara and J. I. Matsuda, *Meteorit. Planet. Sci.*, 2012, **47**, 1728–1737, DOI: **10.1111/maps.12007**.

42 A. Mezzi and S. Kaciulis, *Surf. Interface Anal.*, 2010, **42**, 1082–1084, DOI: **10.1002/sia.3348**.

43 A. Kumar, S. Patil, A. Joshi, V. Bhoraskar, S. Datar and P. Alegaonkar, *Appl. Surf. Sci.*, 2013, **271**, 86–92, DOI: **10.1016/j.apsusc.2013.01.097**.

44 L. Jäntschi, *Appl. Water Sci.*, 2019, **9**(38), 1–11, DOI: **10.1007/s13201-019-0912-1**.

45 J. McMurry, *Organic Chemistry*, Cengage Learning, United States, 2015.

46 D.-H. Wu, H. Huang, M. U. Haq, L. Zhang, J.-J. Feng and A.-J. Wang, *J. Colloid Interface Sci.*, 2023, **647**, 1–11, DOI: **10.1016/j.jcis.2023.05.111**.

47 L.-L. Liu, D.-H. Wu, L. Zhang, J.-J. Feng and A.-J. Wang, *J. Colloid Interface Sci.*, 2023, **639**, 424–433, DOI: **10.1016/j.jcis.20223.02.061**.

48 S.-F. Zhao, L.-X. Wu, H. Wang, J.-X. Lu, A. M. Bond and J. Zhang, *Green Chem.*, 2011, **13**, 3461–3468, DOI: **10.1039/C1GC15929A**.

49 Y. Wang, M. Hatakeyama, K. Ogata, M. Wakabayashi, F. Jin and S. Nakamura, *Phys. Chem. Chem. Phys.*, 2015, **17**, 23521–23531, DOI: **10.1039/C5CP02008E**.

50 N. G. Rey and D. D. Dlott, *J. Phys. Chem. C*, 2015, **119**(36), 20892–20899, DOI: **10.1021/acs.jpcc.5b03397**.

51 H. Wu, J. Song, C. Xie, Y. Hu and B. Han, *Green Chem.*, 2018, **20**, 1765–1769, DOI: **10.1039/C8GC00471D**.

52 S. A. S. Mohammed, W. Z. N. Yahya, M. A. Bustam, M. G. Kibria, A. N. Masri and N. D. M. Kamonwel, *J. Mol. Liq.*, 2022, **359**, 119219, DOI: **10.1016/j.molliq.2022.119219**.

53 D. Das and R. N. Singh, *Int. Mater. Rev.*, 2007, **52**, 29–64, DOI: **10.1179/174328007X160245**.

54 J.-J. Koo, K. H. Jung, K. Park, W. J. Min, K. Yu, Z. H. Kim and J.-K. Lee, *J. Phys. Chem. Lett.*, 2022, **13**(31), 7220–7227, DOI: **10.1021/acs.jpclett.2c01923**.

55 X. Wang and L. Zhang, *RSC Adv.*, 2018, **8**, 40621–40631, DOI: **10.1039/C8RA07880G**.